



ELSEVIER

Available online at www.sciencedirect.com

SCIENCE @ DIRECT®

Nuclear Instruments and Methods in Physics Research B 200 (2003) 315–322

NIM B
Beam Interactions
with Materials & Atomswww.elsevier.com/locate/nimb

Internal stress measurements by high-energy synchrotron X-ray diffraction at increased specimen-detector distance

J. Böhm^a, A. Wanner^{a,*}, R. Kampmann^b, H. Franz^c, K.-D. Liss^b,
A. Schreyer^b, H. Clemens^b

^a *Institut für Metallkunde, Universität Stuttgart, Heisenbergstr. 3, 70569 Stuttgart, Germany*

^b *GKSS-Forschungszentrum Geesthacht GmbH, Institut für Werkstofforschung, Max-Planck-Straße, 21502 Geesthacht, Germany*

^c *Hamburger Synchrotronstrahlungslabor, Deutsches Elektronen-Synchrotron, Notkestr. 85, D-22603 Hamburg, Germany*

Abstract

High-energy X-ray diffraction has recently been shown to be a viable technique to measure volume-averaged lattice strains in the bulk of metallic polycrystals at increased speed compared to neutron diffraction. The established procedure is to irradiate the sample under investigation with monochromatic X-rays (~ 100 keV) and to record complete diffraction rings with an area detector. The lattice strains are obtained by analyzing the minute distortions of these rings. In the present paper we present first results obtained using a setup in which two area detectors are positioned at a large distance (7 m) from the specimen. Although only segments of the rings can be recorded this way, this approach offers a number of advantages. In situ tensile tests were performed on a γ -TiAl-based alloy as an example to demonstrate the potential of the method. Both materials science aspects as well as consequences for further method development will be discussed.

© 2002 Elsevier Science B.V. All rights reserved.

PACS: 07.10.L; 29.20.L; 41.50; 78.70.C

Keywords: Internal stress measurement; Synchrotron X-ray diffraction; Monochromatic high-energy X-rays; Transmission; Grain size

1. Introduction

Many high-performance alloys are multiphase materials. The load-bearing capacity of such materials is controlled by the load transfer between the constituent phases. Experimental measurement of load partitioning between the individual phases can give a wealth of information on the micro-

mechanical evolution during deformation. Classical techniques to measure volume-averaged elastic strains in the bulk of crystalline metallic or ceramic materials are based on diffraction of thermal neutrons. While these techniques have been successful for many applications, typical measurement times are long (in the order of hours) due to the low fluxes available at current neutron sources. The availability of high-energy, high-flux X-rays from third generation synchrotron research facilities offers alternative approaches to diffraction measurements of internal strains which do not have these restrictions and are therefore complementary

* Corresponding author. Tel.: +49-711-6893413; fax: +49-711-6893412.

E-mail address: wanner@mf.mpg.de (A. Wanner).

tools to neutron diffraction [1]. Different techniques for high-energy X-ray strain measurements have been developed. Laue diffraction has successfully been applied for measurements within single crystals or individual grains using focused microbeams (e.g. [2]), Debye–Scherrer diffraction techniques have been developed to obtain volume-averaged results on polycrystalline samples [3–6]. An interesting method with a wide application potential is the high-energy X-ray transmission technique described by Withers and co-workers [4,5] and by Wanner and Dunand [6]. The major setback of this method in its current state of development is, however, that it is limited to fine-grained polycrystals and that it is very sensitive to unintentional specimen movements. Theoretical considerations suggest that these setbacks can be diminished significantly by enlarging the experimental setup by one order of magnitude [7]. An experimental arrangement with two area detectors positioned at a large distance from the sample has recently been established at beamline PETRA2 at Hamburger Synchrotronstrahlungslabor (HASYLAB) [8]. In the present paper we report on first in situ tensile tests carried out at this facility. The measurements were performed on a titanium–aluminide-based alloy of key engineering interest. For comparison, the same tensile tests were also performed using a conventional setup at beamline BW5 at HASYLAB. The main aim of the present study is to explore the capabilities of the improved experimental approach. More results and a deeper discussion concerning the material-specific results will be presented in a subsequent paper.

2. Experimental

2.1. Material

Dog bone-shaped, flat tensile specimens with gauges 50 mm long, 5 mm wide and 1 mm thick, which were fabricated by electric discharge machining and subsequent mechanical polishing, were investigated. The starting sheet material had a nominal composition of Ti–46.5 at.% Al–4 at.% (Cr, Nb, Ta, B) and was fabricated by a powder metallurgical process at Plansee AG (Reutte,

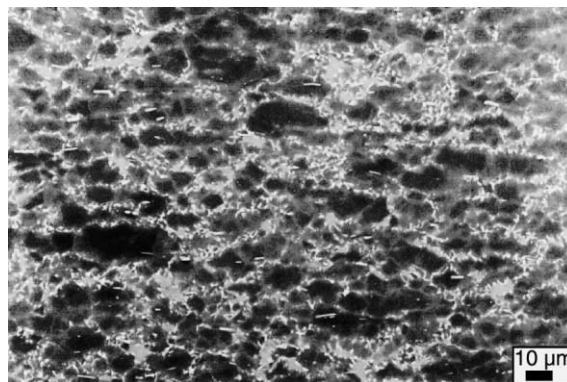


Fig. 1. Microstructure of Ti–46.5 at.% Al–4 at.% (Cr, Nb, Ta, B) sheet material. The two major constituents are γ -TiAl (dark) and α_2 -Ti₃Al (light grey) (back-scattered electron image).

Austria). Details concerning the rolling process and the subsequent heat-treatment in order to flatten the sheet material are comprehensively described in [9]. The obtained “near gamma” microstructure consisted predominantly of equiaxed γ -TiAl (fcc L1₀ structure) grains with an average grain diameter of 15–20 μm (Fig. 1). Approximately 5 vol.% of α_2 -Ti₃Al phase (hex DO₁₉ structure) as well as B2 phase (bcc CsCl structure) were present at grain boundaries and triple points. The rod-like shaped particles are tantalum containing Ti-borides which are preferentially aligned in the rolling direction. A more detailed description of the phases is given in [10].

2.2. Experimental setup

A miniature, screw-driven tensile device was used to perform uniaxial tensile tests at room temperature in situ at either the wiggler beamline BW5 or at the undulator beamline PETRA2 of HASYLAB. In each case the sample under investigation was irradiated in transmission with a monochromatic, parallel high-energy X-ray beam and diffraction patterns were recorded with an area detector. The tensile strain was increased stepwise and held constant during the X-ray exposure. The macroscopic load versus elongation curves were recorded by measuring the crosshead displacement using a linear variable differential transformer (LVDT) and the load using a load cell.

2.2.1. Recording of complete diffraction rings at beamline BW5

In the experiments performed at beamline BW5 the specimen was irradiated with a parallel beam of 100 keV X-rays. The diffraction patterns were recorded using an image-plate detector (Model MAR 345 by MAR, Evanston, IL, USA) positioned ‘on axis’ on the downstream side of the specimen. This detector has a diameter of 345 mm and a pixel size of $0.1 \times 0.1 \text{ mm}^2$. The recorded 16 bit greyscale images had a size of 3450×3450 pixels. The sample to detector distance was 1150 mm, which means that complete diffraction rings could be recorded for diffraction angles up to $\theta = 4.3^\circ$. The spot size of the beam was $0.5 \times 0.5 \text{ mm}^2$ and the exposure time for each image was 150 s. A Fe- or Si-powder calibration substance in a small container was attached to the sample as a reference with a rubber belt. The lattice strains in longitudinal and transverse directions are obtained from the distortions of the diffraction ring relative to the unloaded state based on the following simple relationship:

$$\varepsilon = \frac{d - d_0}{d_0} \approx \frac{D_0 - D}{D}, \quad (1)$$

where d is the lattice spacing, D is the ring diameter and subscript 0 denotes the unloaded state. The experimental setup as well as the evaluation procedure is described in more detail in [6].

2.2.2. Recording of partial diffraction rings at beamline PETRA2

The beamline PETRA2 also offers X-rays in the range of 100 keV. The key advantages over the BW5 station are that (a) the size of the experimental endstation is much larger, thus offering the possibility to position the area detector at a much greater distance (up to 7 m) from the sample [8], and (b) that the beam divergence is substantially smaller ($\leq 50 \mu\text{rad}$ instead of 1 mrad). In order to record complete diffraction rings at such an increased distance, the detector size must be increased accordingly. Since no area detectors with diameters of several meters are available up to now, the measurements must be restricted to selected parts of the pattern. In the present work we positioned the detectors approximately 7 m from

the specimen each recording ring segments for the longitudinal and transverse direction respectively. Partial diffraction patterns of 90 keV photons were recorded using two Xe-gas area detectors [11]. The Xe-detectors were aligned with the direction of their central anode wire parallel to the radius of the diffraction ring to achieve a peak shift resolution of $\sim 0.1 \text{ mm}$ in the 2θ direction. They allow for excellent background subtraction due to their single photon detection mode. The pixel size was 0.3 mm (radial) by 0.5 mm (tangential), and the total sensitive area 300 mm by 300 mm. No calibration substance was used. The boxes marked in Fig. 3 correspond to the area covered by the two detectors. The deformation axis of the miniature tensile device was mounted vertically onto the sample goniometer. The sample was rotated from -0.5° to 0.5° around the horizontal axis perpendicular to the beam. During this tilting operation, a number of 20 frames were stored separately. The frame exposure time was 50 s adding up to a total exposure of 1000 s per loading step. The further analysis in the present paper is based on averaging images obtained by stacking the 20 frames in order to increase the grain statistics. The reflections of individual grains can be investigated in detail by analyzing the sets of single frames, which is the aim of subsequent studies.

3. Results

3.1. Stress–strain curves

The stress–strain curves obtained in the two in situ tensile tests described in the present study are shown in Fig. 2. The yield stress of the alloy is about 525 MPa. Stress relaxation of about 4% is observed in the plastic regime during the holding times in which the X-ray measurements were made. In both tests, specimen fracture occurred at a total strain of about 0.8%.

3.2. X-ray diffraction patterns

Fig. 3 shows part of a typical diffraction pattern recorded using the MAR 345 detector at beamline BW5. For this particular exposure, no calibration

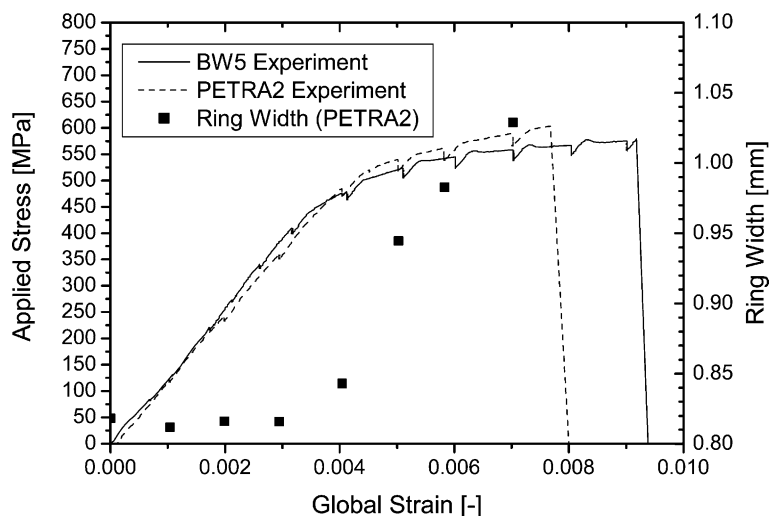


Fig. 2. Macroscopic stress–strain diagrams from two different in situ tensile tests. The kinks in the curves are due to the stress relaxation occurring during hold times. The diagram also shows the evolution of the width of the 222 diffraction ring of the γ phase obtained from the PETRA2 experiment.

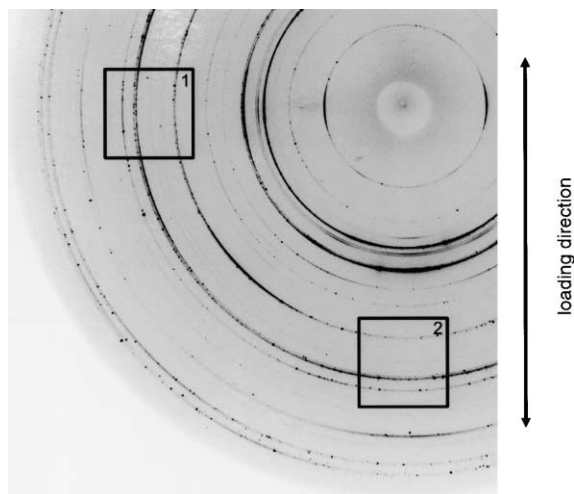


Fig. 3. Part of a typical diffraction pattern of the γ -TiAl-based alloy, recorded by the image plate detector at beamline BW5. A closeup of area “2” is shown in Fig. 4(a).

substance was attached to the specimen. Hence, all of the concentric diffraction rings visible in this figure stem from the alloy. The strong rings belong to the tetragonal phase γ -TiAl, which is the major constituent of the material. The two square-shaped areas delineated in the pattern correspond to the

regions covered by the two area detectors used in the experiments performed at beamline PETRA2. An enlargement of one of the delineated areas is shown in Fig. 4(a). For comparison, a pattern recorded at PETRA2 by one of the two area detectors is shown in Fig. 4(b). This image was obtained by stacking the frames recorded at 20 different tilt angles. It is apparent that the image shown in Fig. 4(b) exhibits a better signal-to-noise ratio and also sharper diffraction rings than Fig. 4(a). More diffraction rings are visible and the doublets stemming from the slight tetragonality of γ -TiAl can be resolved due to the better resolution. A lattice constant ratio of $c/a = 1.012$ was determined by a best fit from the relative positions of the γ -TiAl rings visible in Fig. 4(b).

3.3. Lattice strain evaluation

The elastic strains in the directions parallel to the loading axis (longitudinal direction) and perpendicular to the loading axis (transverse direction) can be deduced from the elliptical distortions of the diffraction rings. If the whole rings are available like in the experiments performed at BW5, the main axes of the ellipse can be obtained by plotting the ring diameter D against $\sin^2 \varphi$,

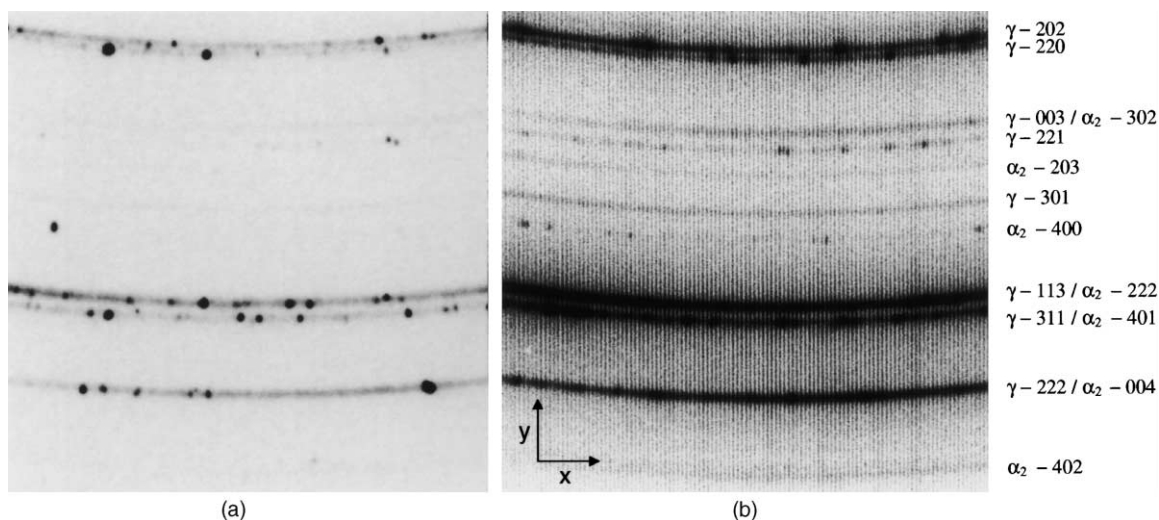


Fig. 4. Corresponding diffraction patterns (a) and (b) registered by the image plate detector at beamline BW5 (area “1” of Fig. 3) and by one of the two wire-frame area detectors at PETRA2, respectively. Reflections are indexed on the right for the phases γ -TiAl and α_2 -Ti₃Al.

where φ is the azimuthal angle. This method is described in detail in [6]. In practice, only some of the diffraction rings visible in Fig. 3 are suitable for strain evaluation. Most of the rings exhibit a too low intensity or they are too close to adjacent diffraction rings. Out of the rings intersecting the square areas delineated in Fig. 3, the 222 ring of the γ -TiAl phase is the only one from which useful

strain results could be obtained. In Fig. 5(a) a D versus $\sin^2 \varphi$ plot for this ring is shown for an applied stress of 470 MPa. For elimination of the apparent strains stemming of unintentional specimen movement, the same evaluation procedure was applied to the 111 diffraction ring of the unstrained Si powder sample attached to the specimen. Fig. 6 shows the net longitudinal and

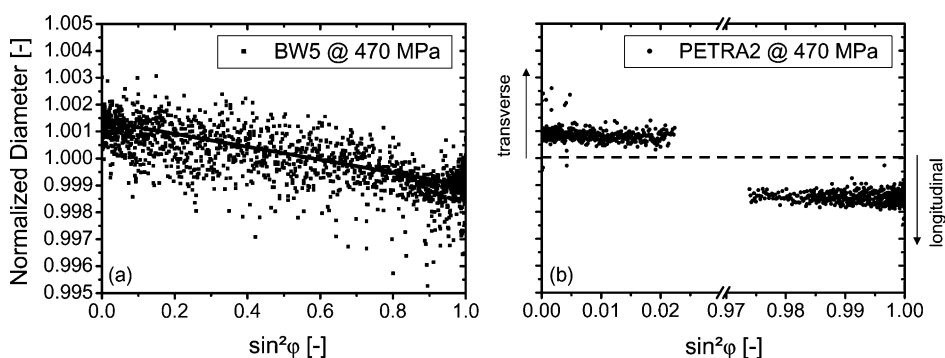


Fig. 5. (a) Example of the strain evaluation procedure based on the full diffraction rings recorded at BW5. The diameter of the γ -TiAl 222 diffraction ring is plotted against $\sin^2 \varphi$, where φ is the azimuthal angle. The diameters are normalized to the average ring diameter in the stress-free starting condition. Due to the lattice strains caused by the applied stress of 470 MPa, the diffraction ring is distorted elliptically. The two main axes of the ellipse are obtained by fitting a straight line to the data and extrapolating to $\sin^2 \varphi = 1$ (longitudinal direction) and $\sin^2 \varphi = 0$ (transverse direction). (b) The same procedure can be applied to the radii of the ring segments recorded at PETRA2. The range of $\sin^2 \varphi$ is restricted to values close to 0 and 1. It is apparent that the data in (b) exhibit considerably less scatter than those in (a).

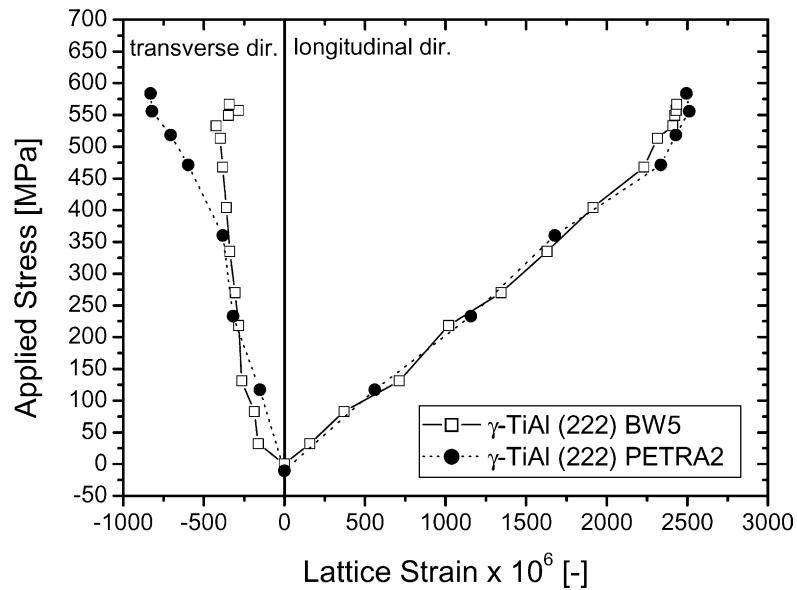


Fig. 6. Applied stress versus lattice strain. The lattice strains were calculated from the distortions of the γ -TiAl 222 diffraction rings or ring segments recorded during in situ tests at beamline BW5 or PETRA2, respectively.

transverse lattice strains derived from the diffraction ring distortions, plotted against the applied stress. The strain results obtained from evaluating the displacements of the 222 ring segments recorded at PETRA2 are also shown. The following improved procedure has been developed in order to obtain the transverse and longitudinal lattice strains from the partial diffraction patterns as recorded by the two detectors: the ring segment of interest is described by the maxima of Gaussian peaks fitted to the intensity data at 500 equispaced x -positions (for coordinate system see Fig. 4(b)). The centre of the undistorted diffraction ring lying far outside the image is calculated by fitting a circle segment to the data set obtained this way. Relative to this centre, the ring diameter D as well as the azimuthal angle φ is calculated for each data point of the ring segment. In Fig. 5(b) these diameters are plotted against $\sin^2 \varphi$, again for an applied stress of 470 MPa. Since the two detectors cover narrow φ -ranges around 0° and 90° , two separate data sets are obtained. One set is used to determine the transverse main axis of the ellipse by extrapolating to $\sin^2 \varphi = 0$, the other one to obtain the longitudinal main axis by extrapolating to

$\sin^2 \varphi = 1$. The changes of these main axes are used to calculate the lattice strains according to Eq. (1).

4. Discussion and conclusions

The applied stress versus lattice strain plot presented in Fig. 6 shows that the data obtained in the two different experiments agree very well, especially in the longitudinal direction. At stresses below 450 MPa (i.e. in the linear-elastic regime according to Fig. 2), the data follow a straight line. The apparent Young's modulus calculated from the slope of this line is 208 GPa, which is close to Young's modulus $E_{111} = 216$ GPa reported for singlecrystalline γ -TiAl [12]. This suggests that in the elastic regime no pronounced load-partitioning exists between the γ -TiAl phase and the other constituents of the alloy.

An apparent Poisson's ratio of $\nu = 0.23$ is obtained by normalising the slope of the straight line describing the experimental transverse strains to the slope of the line describing the longitudinal strains. In order to compare this apparent Pois-

son's ratio to elastic constants reported in literature, we have calculated the normal elastic strains existing in the 111 direction of an *isolated*, unconstrained γ -TiAl single-crystal parallel subjected to uniaxial stress in either the 111 direction, the $1\bar{1}0$ direction, or the $11\bar{2}$ direction. These three directions are nearly orthogonal since the c/a lattice constant ratio of γ -TiAl is close to unity. Using the single-crystal elastic constants reported in [13], the computations yield the following results:

$$\varepsilon_{111}^{111} = 0.46 \times 10^{-11},$$

$$\varepsilon_{111}^{110} = 0.12 \times 10^{-11},$$

and

$$\varepsilon_{111}^{112} = 0.05 \times 10^{-11}.$$

The two Poisson's ratios which can be defined based on these elastic strains are

$$\nu_{111}^{110} = -\varepsilon_{111}^{110}/\varepsilon_{111}^{111} = 0.26$$

and

$$\nu_{111}^{112} = -\varepsilon_{111}^{112}/\varepsilon_{111}^{111} = 0.10,$$

which shows that a wide distribution of Poisson's ratios is expected for the individual grains in the polycrystal. The apparent Poisson's ratio measured experimentally ($\nu = 0.23$, see above) is the effective value of a large number of grains.

The deviation from linearity observed at higher stresses in Fig. 6 indicates that load transfer from the 111 γ -TiAl grains to other constituents takes place in the plastic regime. The deviation between the two transverse strain curves observed at high applied stresses is not clear. For a more detailed analysis of this process it is, however, required to measure the lattice strains in γ -TiAl-grains with other orientations and in the other phases of the alloy, which will be the aim of further investigation. To this end, advanced algorithms to evaluate the displacements of all of the ring segments visible in Fig. 4(b) are being developed. The main challenge here is to overcome the problems arising from a low signal-to-noise ratio and from small distances between adjacent rings. The results of the present study have demonstrated that the enlarged

experimental setup realized at PETRA2 offers a wide potential for micromechanical studies on polycrystalline materials. The disadvantages from not being able to record the full diffraction rings are more than compensated by the better resolution of the partial patterns recorded at a greater distance from the specimen. The substantially increased specimen-to-camera distance also diminishes the effects of unintentional specimen movements on the lattice strain results, which is why measurements can be made without a calibration substance. This will facilitate future experiments significantly, especially if elevated testing temperatures are involved.

Acknowledgements

Financial support by the Deutsche Forschungsgemeinschaft (DFG), Bonn, Germany, through Project No. SFB381/A1 is gratefully acknowledged. The diffraction measurements were carried out at beamlines BW5 and PETRA2 of the Hamburger Synchrotronstrahlungslabor (HASYLAB) at Deutsches Elektronen-Synchrotron (DESY), Hamburg, Germany. We thank HASYLAB staff for their excellent technical support.

References

- [1] A. Pyzalla, W. Reimers, K.-D. Liss, Mater. Sci. Forum 347–349 (2000) 34.
- [2] H. Biermann, B.V. Grossmann, S. Mechsner, H. Mugh-rabi, T. Ungar, A. Snigirev, I. Snigireva, A. Souvorov, M. Kocsis, C. Raven, Scr. Mater. 37 (1997) 1309.
- [3] A. Royer, A. Jacques, P. Bastie, M. Veron, Mater. Sci. Eng. A A319–321 (2001) 800.
- [4] M.R. Daymond, P.J. Withers, Scr. Mater. 35 (1996) 1229.
- [5] A.M. Korsunsky, K.E. Wells, P.J. Withers, Scr. Mater. 39 (1998) 1705.
- [6] A. Wanner, D.C. Dunand, Metall. Mater. Trans. A 31A (2000) 2949.
- [7] A. Wanner, D.C. Dunand, J. Neutron Res. 9 (2001) 495.
- [8] R. Kampmann, T. Lippmann, J. Burmester, J.F. dos Santos, H. Franz, M. Haese-Seiller, M. Marmotti, Nucl. Instr. and Meth. A 467/468 (2001) 1261.
- [9] H. Clemens, H. Kestler, N. Eberhardt, W. Knabl, in: Y.-W. Kim, D.M. Dimiduk, M.H. Loretto (Eds.), Processing of γ -TiAl-Based Alloys on an Industrial Scale,

- Gamma Titanium Aluminides 1999, TMS, Warrendale, PA, 1999, p. 209.
- [10] B.J. Inkson, H. Clemens, Mater. Res. Soc. Symp. Proc. 552 (1999) KK3.12.
- [11] M. Marmotti, J. Burmeister, M. Haese-Seiller, R. Kampmann, Nucl. Instr. and Meth. A 477 (2002) 347.
- [12] Y. He, R.B. Schwarz, A. Migliori, J. Mater. Res. 10 (1995) 1187.